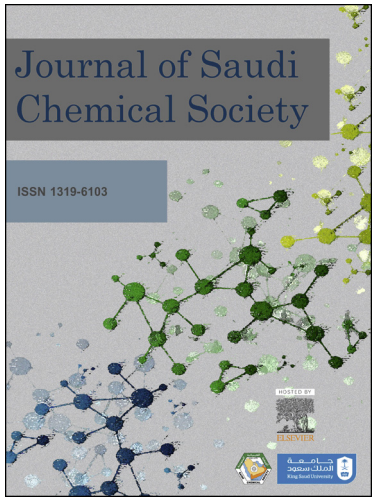

Original article

Investigation of the growth parameters of hydrothermal ZnO nanowires for scale up applications

Naif Ahmed Alshehri, Aled R. Lewis, Cameron Pleydell-Pearce, Thierry G.G. Maffeis

PII: S1319-6103(17)30111-4
DOI: https://doi.org/10.1016/j.jscs.2017.09.004
Reference: JSCS 911

To appear in: *Journal of Saudi Chemical Society*

Received Date: 23 July 2017
Revised Date: 11 September 2017
Accepted Date: 18 September 2017

Please cite this article as: N. Ahmed Alshehri, A.R. Lewis, C. Pleydell-Pearce, T.G.G. Maffeis, Investigation of the growth parameters of hydrothermal ZnO nanowires for scale up applications, *Journal of Saudi Chemical Society* (2017), doi: https://doi.org/10.1016/j.jscs.2017.09.004

Investigation of the growth parameters of hydrothermal ZnO nanowires for scale up applications

Naif Ahmed Alshehri[1,2], Aled R Lewis[1], Cameron Pleydell-Pearce[3] and Thierry G. G. Maffeis[1]

Corresponding author: Naif Alshehri

80834@swansea.ac.uk

Aled Lewis

557952@swansea.ac.uk

Cameron Pleydell-Pearce

c.pleydell-pearce@swansea.ac.uk

Corresponding author: Thierry Maffeis

t.g.g.maffeis@swansea.ac.uk

[1]Multidisciplinary Nanotechnology Centre at Swansea University, Swansea, United Kingdom

[2]College of science physics department at Albaha University, Albaha, Saudi Arabia

[3]Advanced Imaging of Materials, Engineering, Swansea University, Swansea, United Kingdom

Abstract

Zinc oxide nano-wires (ZnO NWs) are synthesized reproducibly with high yield via a low temperature hydrothermal technique. The influence of the growth duration time, growth temperature, zinc precursor and base concentration of Na_2CO_3 on the morphology of NWs is investigated. The growth products are characterised using scanning electron microscopy (SEM), Transmission electron microscopy (TEM), X-ray diffraction (XRD), X-ray photoelectron spectroscopy (XPS) and photoluminescence (PL). SEM analysis shows that the optimum growth temperature is 140 °C and finds that length and diameter of ZnO NWs have a relationship with growth duration time and base concentrations of Na_2CO_3. In addition, it is reported that a high (~ 90%) yield of ZnO NWs can be synthesised via using any of three different precursors: zinc chloride, zinc acetate and zinc nitrate. TEM and XRD results indicate the high purity and the single crystalline nature of the ZnO NWs. XPS confirms the absence of sodium contaminants on the surface and indicates a near flat band surface condition. PL shows a large visible band in the yellow part of the spectrum, and a small

exciton emission peak, indicating a large defect concentration, which is reduced after annealing in air.

Keywords Semiconducting materials; Nanomaterials; Hydrothermal crystal growth; Characterization; X-ray diffraction; Defects.

1. Introduction

Low cost, high yield and controlled fabrication are key factors to realizing the potential of nanomaterials band gap [1, 2], and a high exciton binding energy of 60 meV at room temperature [3-5]. ZnO nanostructures such as nanowires and nanorods are ideal building blocks for many applications due to the unique properties of ZnO, their large surface area to volume ratio [4], and the ability to grow several single crystal geometries.

In recent years, different methods have been used to synthesis ZnO nanowires including vapour liquid solid (VLS) growth [6, 7], metal organic chemical vapour deposition (MOCVD) [7, 8], microemulsion synthesis [9], solvothermal [10] and hydrothermal methods [3]. Amongst all of these methods, hydrothermal growth has attracted a lot of interest because of its many advantages including low cost, low temperature, high yield [3], scalability, and ease of handling. A plethora of nano ZnO shapes have been fabricated using hydrothermal methods including nanobelts, nanowires, nanoflowers and nanoparticles. Hierarchical structures are of particular interest because of their very high surface to volume ratio which has been shown to significantly increase the power conversion efficiency of solar cell [11-13].

ZnO NWs has been grown hydrothermally either in a colloidal form [3, 14] or from a seed layer on various substrates[15-19]. Various studies have found that the growth parameters such as growth duration time [18, 20, 21], growth temperature [22]and precursor concentration [23], have a huge impact on the aspect ratio [3], nanoparticle size [24] and nanowire density [15]. Recent hydrothermal methods have been developed to directly grow NWs at a specific location by localized heat source or using seed patterning. For localized heat, two main process have been used including focused energy field synthesis which relies on Joule heating [25, 26] and laser-induced hydrothermal growth [27-31]. For the seed patterning, methods include microcontact printing of seed nanoparticles [32], inkjet-printed seed patterning [33] and inkjet-printed zinc precursor [34]. These novel methods do not

require expensive photolithography or vacuum deposition and their development widens the range of ZnO NW applications due to their low-temperature synthesis, low cost, environmentally friendly, and simple process setup. Therefore, they can be applied to different types of substrates and can be scaled up for mass production. However, the growth of NWs in a colloidal form is still essential for more versatile applications.

The ZnO NWs studied in this paper are grown using a simple colloidal growth technique first published by Hu et al [3]. In their paper they use a supersaturated solution of Na_2CO_3 to fabricate NWs over 12 h at 140°C using zinc chloride as precursor. In this paper, we demonstrate the reproducibility of the method and explore the parameter space further, highlighting the high yield of the technique and therefore its potential for scaling up NW fabrication to commercial level. The parameters investigated include the concentration of Na_2CO_3, growth duration time, the growth temperature and zinc precursors. Additionally, we show that ZnO NWs can be synthesized not only using zinc chloride as precursor salt but also using zinc acetate dihydrate and zinc nitrate hexahydrate. The effect of annealing the grown NWs in air is also studied using characterization techniques not employed in the original paper such as x-ray photoelectron spectroscopy (XPS) and photoluminescence spectroscopy (PL).

2. Experimental procedure

Zinc chloride ($ZnCl_2$), zinc nitrate hexahydrate ($Zn(NO_3)_2 \cdot 6H_2O$), zinc acetate dihydrate ($Zn(CH_3COO)_2 \cdot 2H_2O$)) and sodium carbonate (Na_2CO_3) were purchased from Sigma Aldrich and used without further purification. The filter paper was purchased from Merck Millipore. In a typical experiment, 0.267 g $ZnCl_2$ (~ 0.032 M), and 26.67 g Na_2CO_3 (~4.193 M) were added to a beaker and topped up to 60 mL with deionized water (DI) and stirred at room temperature for 10 minutes. The solution was transferred into a 125 mL Teflon vessel, which was then sealed in an autoclave. The autoclave was placed in an oven and heated to 140 °C for 3 to 26 hours and then cooled down to room temperature naturally. The resulting white products were washed with 8 L of DI water and vacuum filtered using a hydrophilic nylon membrane with a 1.2 µm pore size. Finally, the filtered white products were dried in a desiccator jar for several hours. To obtain a suspension the dried powder sample was sonicated in DI water in an ultrasonic bath for 10 minutes. The experimental procedure using the other precursor salts is identical, keeping the molarity constant at ~0.032 M. The morphology and size of the ZnO products were characterised using a Hitachi model S-4800 II field-emission scanning electron microscope (FE SEM). To

measure the length and diameter of NWs several images were taken by SEM at the same magnification (5k for length measurements and 100k for diameter). 100 NWs were chosen randomly from each sample and measured using Image J. Averages, standard deviation and error bars were then calculated (the error bars are 2 standard errors wide). The ZnO NWs crystallinity was examined via a Bruker D8 Discover X-ray diffraction (XRD) system. High resolution Transmission Electron Microscopy (HRTEM) was used to observe the morphology and lattice spacing of the ZnO NWs. The surface chemistry and surface band bending was investigated using a Kratos Supra XPS and the photoluminescence spectra recorded using an Ocean optics USB2000+ spectrometer and a Melles-Griot 325 nm He-Cd laser as the excitation source.

3. Results and discussion

3.1. X-ray diffraction and Transmission electron microscopy results

The crystal structure of ZnO NWs was analysed by powder XRD and TEM. A typical XRD pattern is shown in Fig1. The strongest peaks observed at 2θ values of 31.7, 34.4, 36.2, 47.5, 56.5, 62.8, 66.3, 67.9 and 69.1 are corresponding to the lattice planes of (100), (002), (101), (102), (110), (103), (200), (112) and (201) respectively. All of these diffraction peaks are assigned to a ZnO hexagonal wurtzite structure and are matched with reported data for ZnO (a = 3.249A°, c = 5.205A° JCPDS File, 5-664) [3, 35-37]. Furthermore, no diffraction peaks from Zn or other impurities are observed in the pattern which indicates the high purity of ZnO NWs. High resolution TEM images of a single ZnO NWs are shown in Fig 2. Fig 2(b) shows that the average distance between the lattice planes is 0.26 nm which corresponds to the (0002) plane [38, 39] and therefore a c-axis growth direction.

3.2. Effect of Temperature

The effect of temperature was not reported in the original paper. Here we fixed the concentration of Na_2CO_3 at 4.193 M, the growth time at 6 hours and kept ZnCl□ as the precursor salt. Separate growth runs were conducted at 120°C, 140°C and 160°C, and the corresponding SEM images of the growth products are shown in Fig 3**.** Nanowires with diameter of approximately 50 nm and length in excess of 1 µm are only obtained during the 140°C growth. At 120°C, larger crystals with diameter greater than 400 nm and length of 1-2 µm with rough surfaces are produced whilst 160°C yielded predominantly multipod type structures with several large crystals, again with diameter greater than 400 nm, growing out of a common nucleation site. The difference in size of the growth products between 120°C and 140°C is illustrated by the photographs in the insets of Fig3 (a, b) showing that

sedimentation of the suspended growth products 15 mins after suspension is much less at 140°C than at 120°C.

3.3. Effect of growth duration time

NWs were successfully grown at different duration times of 3, 6, 9, 12,16 and 26 h with all other parameters remaining constant (140°C with 4.193 M Na_2CO_3 and 0.032 M $ZnCl_2$). Detailed analysis of the SEM measurements is shown in Fig 4(a). The average ZnO NWs length increases with growth duration time from 1.1 μm (3h) to 3.3 μm (26h), whilst the average diameter of the ZnO NWs remains statistically constant at around 41 nm. The length of the NWs obtained after 26 h was not statistically different than the length of the 16 h NWs. This could be explained by the fact that all the free Zn^{2+} in the solution have been consumed. However , the fact that the yield approaches 100% after 6h indicates that the free Zn^{2+} ions supply is already running out after 6 h. Therefore the continuing increase in length with time could be attributed to an Ostwald ripening process where small NWs dissolve and larger NWs keep growing until the process reaches equilibrium after 16 h. The same trend with growth duration time was observed for another set of samples prepared with a lower concentration of 3.145 M Na_2CO_3 and a temperature of 140 °C (not shown). These results suggest that the growth occurs almost exclusively along the c axis once the initial nucleation has occurred. The main reason is likely to be the very high concentration of Na_2CO_3. We have shown that there is a clear link between increasing Na_2CO_3 concentration and decreasing NW diameter. This is possibly a consequence of the alkaline condition induced by the Na_2CO_3 (pH of 11.5). Joo *et al* [40] have shown that at pH 11, the (1120) side facets of the ZnO NWs become positively charged and the (0001) end facets become negatively charged, resulting in the suppression of lateral growth. It is likely that this mechanism is also responsible for our observations.

3.4. Effect of base concentration (Na_2CO_3)

Na_2CO_3 supersaturation of the solution is an important factor for the nucleation and growth of ZnO NWs [3]. The role of Na_2CO_3 is still unclear but it acts as a weak base which slowly hydrolyses in the water solution and gradually produces OH^- [3]. We attempted growth using the following Na_2CO_3 concentrations including 2.044 M, 2.673 M, 3.145 M, 4.193 M and 4.717 M keeping all other parameters constant (140 °C and 6 h). At the lowest concentration of 2.044 M, NWs are not fabricated and only micrometre size crystals are forming, as shown

in Fig 5 (a). When the concentration increases to 2.673 M a mix of NWs and large crystal are obtained as shown in Fig 5 (b). At 3.145 M, 4.193 M and 4.717 M, NWs are successfully fabricated as shown in Fig 5 (c, d and f) respectively. Since the solubility of Na_2CO_3 at 140 °C is 28.1% by mass [41], the lowest concentration of 2.044 M is below the saturation conditions (21.6% by mass). 2.673 M corresponds to the saturation level with 28.3% by mass and other concentrations including 3.145 M, 4.193 M and 4.717 M are supersaturation solutions with 33.3 % by mass, 44.45 % by mass and 50 % by mass respectively. Based on the above analysis, any concentration below 2.673 M is not able to form ZnO NWs, any concentration above 2.673 M results in supersaturation and hence NWs are synthesized. This is in good agreement with the original paper by Hu et al. However, unlike Hu et al., the formation of nanobelts are not observed. Additionally, our results show that the aspect ratio of the NWs produced is dependent on the base concentration. Fig 4(b) shows that the average length of the NWs increased, whilst the average diameter decreased as the concentration of Na_2CO_3 increased from 2.673 M to 4.717 M. The length increased from 1.7 µm (2.673 M) up to 2.7 µm (4.717 M), while the diameter decreased from 60.7nm (2.673 M) down to 40.9 nm (4.717 M). Further addition of Na_2CO_3 (i.e. above 4.717 M), does not dissolve in the solution and therefore has no effect on the NWs. As mentioned earlier we attribute the decrease in diameter to the increased pH , causing the side facets to become positively charged and suppressing lateral growth.

3.5. Effect of zinc salt precursor

The effect of altering the zinc precursor was also investigated by replacing zinc chloride with zinc nitrate hexahydrate, and zinc acetate dehydrate. All other growth conditions were kept constant: concentration of Na_2CO_3 at 4.193 M, the growth time at 6 h, the growth temperature at 140 °C and concentration of zinc precursors kept at the same molarity of 0.032 M. The corresponding SEM images of the growth products are shown in Fig 6 (a, b and c). SEM images show that NWs are obtained with all three zinc precursor used. Analysis of the SEM measurement is shown in Fig 6. It can be seen that NWs have approximately the same length and diameter which means that the zinc salt precursors do not have a significant impact on the aspect ratio or morphology of NWs.

3.6. ZnO nanowires yield

Fig 5(f) shows a digital photograph of the nanowires lifted off the filtration membrane after washing, filtration and drying in a desiccator. The filtered products for three identical growth runs (3.145 M Na_2CO_3, 0.032 M $ZnCl$□, 140 °C and 6 h) were weighed and an average

weight of 142.8 mg of ZnO nanowires was obtained, which correspond to an atomic yield of nearly 90%; i.e. 9 out of 10 zinc atoms provided by the precursor were used to produce ZnO nanowires. This remarkable high yield, associated with the low cost of the chemicals and the ease of fabrication, makes this method very favourable for scale up operations.

3.7. X-ray photoelectron spectroscopy results

The XPS survey scan in Fig 7 showed the expected Zn, O and C peaks and demonstrates the purity of the sample after rinsing and filtering as no Na peak is present in spite of the high concentration of Na_2CO_3 during the growth. Percentage composition of the O1s core level, Zn 2p and C 1s as a function of annealing temperatures in air are shown in table 1**,** extracted from the curve fitting of each core level. The O1s core level peak shape is shown in Fig 8 and fitted with two components**.** The first peak at 530.7 eV is attributed to O^{2-} oxidation state bound with Zn in the crystal lattice and the high binding energy peak at 532 eV corresponds to surface oxygen species such as OH^- ions[42-45]. Table 1 indicates that there is a significant reduction in surface carbon and surface oxygen with temperature. The zinc to lattice oxygen ratio decreased from 1.145 to almost 1 following the last anneal indicating that annealing resulted in a reduction of oxygen vacancies. In addition, XPS valence band spectra shown on Fig 9 reveal a near flat band condition with the valence band edge 3.1eV below the Fermi level, which was unaffected by the anneals.

3.8. Photoluminescence results

The PL spectra of NWs grown for 3, 6, 9, and 12 h are shown in Fig 10, as well as the spectrum of the 3h NWs after annealing at 400 °C**.** The spectra were normalized to the excitonic, near band edge (NBE) peak at 376 nm in the main graph and to the deep level emission (DLE) band in the inset. The DLE band is thought to originate from several radiative transitions between the band edges and deep levels caused by oxygen vacancies and interstitials[46-50]. The main graph shows that the DLE peaks increase in intensity compared to the NBE peak with growth duration time but there is no change in the shape of either peak. This suggests that the efficiency of radiative recombination through deep levels appears to increase with growth duration time, compared to exciton recombination. The shape of the

DLE band, with an intensity maximum near 600nm is also very similar to previously reported results on vertical ZnO NWs arrays [51]. Annealing the 3h sample at 400°C (inset of Fig 10) increases the intensity of the NBE peak relative to the DLE band by a factor of 4. The anneal also causes the DLE band shape to change, with the peak maximum shifting from 600 nm to 640 nm, indicating that the lowest wavelength defect assisted transition is decreased by the anneal compared to the other contributions to the DLE. The shape of the DLE band after annealing at 400°C is also very similar to that observed on ZnO nanosheets produced by annealing zinc acetate at 400°C in air [47, 52], indicating that the effect of this anneal are reproducible on different ZnO nanomaterials. Both the increase in NBE emission and the change in shape of the DLE band were also observed on the 12h sample following annealing at 400°C (not shown). It can be concluded that the anneal removes defects, improving crystallinity. This is in good agreement with the XPS showing a reduction in oxygen vacancies.

4. Conclusion

The growth parameters (temperature, duration time and base concentration) of a low temperature hydrothermal method for producing ZnO NWs with controllable length and diameter have been investigated. The optimum growth temperature was found to be centred around 140°C. Increasing the growth duration time increases the length of the grown ZnO NWs but does not have a significant impact on the NWs diameter. Increasing the base concentration increases the aspect ratio of the NWs. Three different salt precursors were used with no significant difference in the growth products. The yield was measured at around 90%. XPS investigation shows effective removal of surface contamination of ZnO NWs annealed in air up to 400°C and a reduction in oxygen lattice vacancies. XPS also indicated near flat band conditions at the surface, unaffected by air annealing. Finally, PL shows that the 400°C anneal removes defects, improving the intrinsic optical properties of the material. This method is simple, low cost, requires no harmful chemicals and possesses a very high yield and so could offer a viable route for the scaled up production of ZnO NWs with controllable aspect ratios.

Acknowledgement

Naif Alshehri acknowledges the financial support through Al-Baha University in Saudi Arabia.

References

[1] Demes T, Ternon C, Riassetto D, Stambouli V, Langlet M 2016 Comprehensive study of hydrothermally grown ZnO nanowires *J. Mate. Sci*. **51** 10652-61

[2] Bai S-N 2012 Growth and properties of ZnO nanowires synthesized by a simple hydrothermal method *J. Mater. Sci. Mater Electron.* **23** 398-402

[3] Hu H, Huang X, Deng C, Chen X, Qian Y 2007 Hydrothermal synthesis of ZnO nanowires and nanobelts on a large scale *Mater. Chem. Physics.* **106** 58-62

[4] Jagadish C and Pearton SJ 2011 *Zinc Oxide Bulk, Thin Films and Nanostructures: Processing, Properties, and Applications* Elsevier Science

[5] Bagnall DM et al 1997 Optically pumped lasing of ZnO at room temperature *Appl. Phys. Lett*. **70** 2230-2

[6] Petersen EW, Likovich EM, Russell KJ, Narayanamurti V 2009 Growth of znO nanowires catalyzed by size-dependent melting of au nanoparticles *Nanotechnology*. **20** 405603

[7] Gomez JL, Tigli O 2013 Zinc oxide nanostructures: from growth to application *J. Mater. Sci* **48** 612-24

[8] Protasova L et al 2011 ZnO based nanowires grown by chemical vapour deposition for selective hydrogenation of acetylene alcohols *Cata. Sci. Technol.* **1** 768-77

[9] Lim S, Hwang S, Kim S 2010 Microemulsion synthesis and characterization of aluminum doped zno nanorods *Cryst. Res. Technol.* **45** 771-5

[10] Cheng H-M, Chiu W-H, Lee C-H, Tsai S-Y, Hsieh W-F 2008 Formation of branched ZnO nanowires from solvothermal method and dye-sensitized solar cells applications *J. Phys. Chem. C.* **112** 16359-64

[11]Herman, I, et al, 2012 Hierarchical weeping willow nano-tree growth and effect of branching on dye-sensitized solar cell efficiency *Nanotechnology* **23** 194005

[12] Wanit, M, et al, 2012 ZnO nano-tree growth study for high efficiency solar cell *Energy Procedia* **14** 1093-98

[13] Ko, S.H, et al, 2011 Nanoforest of hydrothermally grown hierarchical ZnO nanowires for a high efficiency dye-sensitized solar cell *Nano letters* **11** 666-71

[14] Cheng W-Y, Lin Y-F, Lu S-Y 2011 Nanowires improved charge separation and light utilization in metal-oxide solar cells *Appl. Phys. Lett.* **99** 063107

[15] Xu S, Lao C, Weintraub B, Wang ZL 2008 Density-controlled growth of aligned ZnO nanowire arrays by seedless chemical approach on smooth surfaces *J. Mater. Res.* **23** 2072-7

[16] Robak E, Coy E, Kotkowiak M, Jurga S, Zaleski K, Drozdowski H 2016 The effect of cu doping on the mechanical and optical properties of zinc oxide nanowires synthesized by hydrothermal route *Nanotechnology*. **27** 175706

[17] Yang J et al 2010 Oriented growth of ZnO nanostructures on different substrates via a hydrothermal method *J. Alloys Compd* **489** 51-5

[18] Han Z, Li S, Chu J, Chen Y 2013 Controlled growth of well-aligned zno nanowire arrays using the improved hydrothermal method *J. Semicond.* **34** 063002

[19] Bai S-N, Wu S-C 2011 Synthesis of ZnO nanowires by the hydrothermal method, using sol–gel prepared ZnO seed films *J Mater Sci. Mater Electron* **22** 339-44

[20] Yuan Z, Yu J, Wang N, Jiang Y 2011 Well-aligned zno nanorod arrays from diameter-controlled growth and their application in inverted polymer solar cell *J. Mater. Sci-Mater El.* **22** 1730-5

[21] Baruah S, Dutta J 2009 Effect of seeded substrates on hydrothermally grown ZnO nanorods *J. Sol-Gel. Sci. Technol.* **50** 456-64

[22] Sugunan A, Warad HC, Boman M, Dutta J 2006 Zinc oxide nanowires in chemical bath on seeded substrates: role of hexamine *J. Sol-Gel Sci Technol.* **39** 49-56

[23] Amin G, Asif MH, Zainelabdin A, Zaman S, Nur O, Willander M 2011 Influence of ph, precursor concentration, growth time, and temperature on the morphology of zno nanostructures grown by the hydrothermal method *J. Nanomate.* **2011** 9

[24] Mayekar J, Dhar V, Radha S 2014 Role of salt precursor in the synthsis of zinc oxide nanparticles *Int. J. Res. Eng. Technol.* **44** 2319-1163

[25] Yang, D, et al, 2015 Focused energy field method for the localized synthesis and direct integration of 1D nanomaterials on microelectronic devices *Advanced Materials* **27** 1207-15

[26] Yeo, J, et al, 2014 Single Nanowire Resistive Nano□heater for Highly Localized Thermo□Chemical Reactions: Localized Hierarchical Heterojunction Nanowire Growth. *Small* **10** 5015-22

[27] In, J.B, et al, 2014 In Situ Monitoring of Laser□Assisted Hydrothermal Growth of ZnO Nanowires: Thermally Deactivating Growth Kinetics *Small* 2014 **10** 741- 49

[28] Hong, S, et al, 2013 Low-temperature rapid fabrication of ZnO nanowire UV sensor array by laser-induced local hydrothermal growth *Journal of Nanomaterials* **2013** 2

[29] Hong, S, et al, 2013 Digital selective growth of a ZnO nanowire array by large scale laser decomposition of zinc acetate *Nanoscale* **5** 3698 -703

[30] Yeo, J, et al, 2013 Rapid, one□step, digital selective growth of ZnO nanowires on 3D structures using laser induced hydrothermal growth *Advanced Functional Materials* **23** 3316-23

[31] Yeo, J, et al, 2015 Laser-induced hydrothermal growth of heterogeneous metal-oxide nanowire on flexible substrate by laser absorption layer design *ACS nano* **9** 6059-68

[32] Kang, H.W, et al, 2011 Simple ZnO nanowires patterned growth by microcontact printing for high performance field emission device *The Journal of Physical Chemistry C* **115** 11435-41

[33] Ko, S.H, et al, 2011 Digital selective growth of ZnO nanowire arrays from inkjet-printed nanoparticle seeds on a flexible substrate *Langmuir* **28** 4787-92

[34] Kwon, J, et al, 2013 Direct selective growth of ZnO nanowire arrays from inkjet-printed zinc acetate precursor on a heated substrate *Nanoscale research letters* **8** 489

[35] Fang G, Li D, Yao B-L. 2003 Fabrication and characterization of transparent conductive ZnO:Al thin films prepared by direct current magnetron sputtering with highly conductive ZnO(ZnAl2O4) ceramic target. *J. Cryst. Growth*. **247** 393-400

[36] Hu H, Deng C, Huang X. 2010 Hydrothermal growth of center-hollow multigonal star-shaped ZnO architectures assembled by hexagonal conic nanotubes *Mater .Chem. Phys.* **121** 364-9

[37] Zhang J, Yu W, Zhang L. 2002 Fabrication of semiconducting ZnO nanobelts using a halide source and their photoluminescence properties *Phys. Lett A*. **299** 276-81

[38] Kamble AS et al 2014 Effect of hydroxide anion generating agents on growth and properties of ZnO nanorod arrays *Electrochim. Acta* **149** 386-93

[39] Huang X, Shao L, She G-W, Wang M, Chen S, Meng X-M 2012 Catalyst-free synthesis of single crystalline ZnO nanonails with ultra-thin caps *CrystEngComm* **14** 8330-4

[40] Joo, J, et al 2011 Face-selective electrostatic control of hydrothermal zinc oxide nanowire *synthesis Nature materials* **10** 596

[41] Waldeck WF, Lynn G, Hill AE 1932 Aqueous solubility of salt at high tempertures. I. solubility of soduim carbonate from 50 to 348°1 *J. Am. Chem. Soc*. **54** 928-36

[42] Zhong J, Cheng K, Hu B, Gong H, Zhou S, Du Z 2009 Temperature-controlled growth and optical properties of zno nanorods with quadrangular and hexagonal cross sections *Mater. Chem. Phys.* **115** 799-803

[43] Huang Q et al 2015 HAZO/AZO structure with improved full spectrum performance for high-efficiency thin-film solar cells *Sol. Energ. Mat. Solc. C.* **136** 11-6

[44] Maffeis TGG, Penny MW, Castaing A, Guy OJ, Wilks SP. 2012 XPS investigation of vacuum annealed vertically aligned ultralong ZnO nanowires *Surf. Sci*. **606** 99-103

[45] Jin Y, Cui Q, Wen G, Wang Q, Hao J, Wang S, et al. 2009 XPS and Raman scattering studies of room temperature ferromagnetic ZnO: Cu *Journal of Physics D: Appl. Phys*. **42** 215007

[46] Djurišić A et al. 2007 Defect emissions in ZnO nanostructures. *Nanotechnology*. **18** 095702

[47] Barnett CJ, Smith NA, Jones DR, Maffeis TGG, Cobley RJ. 2015 Effects of Vacuum Annealing on the Conduction Characteristics of ZnO Nanosheets *Nanoscale Res Lett.* **10** 6

[48] Liao Z-M, Zhang H-Z, Zhou Y-B, Xu J, Zhang J-M, Yu D-P. 2008 Surface effects on photoluminescence of single ZnO nanowires *Phys. Lett A.* **372** 4505-9

[49] Janotti A, Van de Walle CG. 2005 Oxygen vacancies in ZnO *Appl. Phys. Lett.* **87** 122102

[50] Gao J, Zhang X, Sun Y, Zhao Q, Yu D. 2010 Compensation mechanism in N-doped ZnO nanowires *Nanotechnology*. **21** 245703

[51] Brown RA et al 2013 The effect of metal layers on the morphology and optical properties of hydrothermally grown zinc oxide nanowires *J. Mater. Sci* **48** 4908-13

[52] Tarat A et al 2014 Microwave-assisted synthesis of layered basic zinc acetate nanosheets and their thermal decomposition into nanocrystalline ZnO *Nanoscale Res Lett.* **9** 11

Table 1: Percentage composition of the O1s core level, Zn and C 1s as a function of annealing temperatures in air

Annealing Temperature °C	Oxygen lattice	Oxygen surface	Zinc	Carbon	Zinc/ lattice Oxygen
70	20.54	25.99	23.52	29.95	1.145
200	24.90	21.55	26.85	26.7	1.078
300	28.84	19.92	29.71	21.54	1.030
400	31.38	20.19	31.50	16.92	1.003

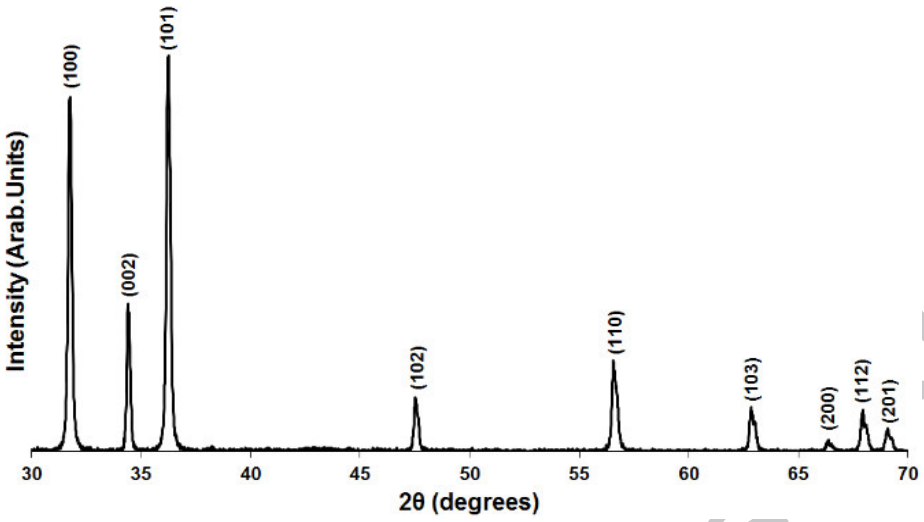

Fig. 1 XRD patterns recorded from the ZnO nanowires

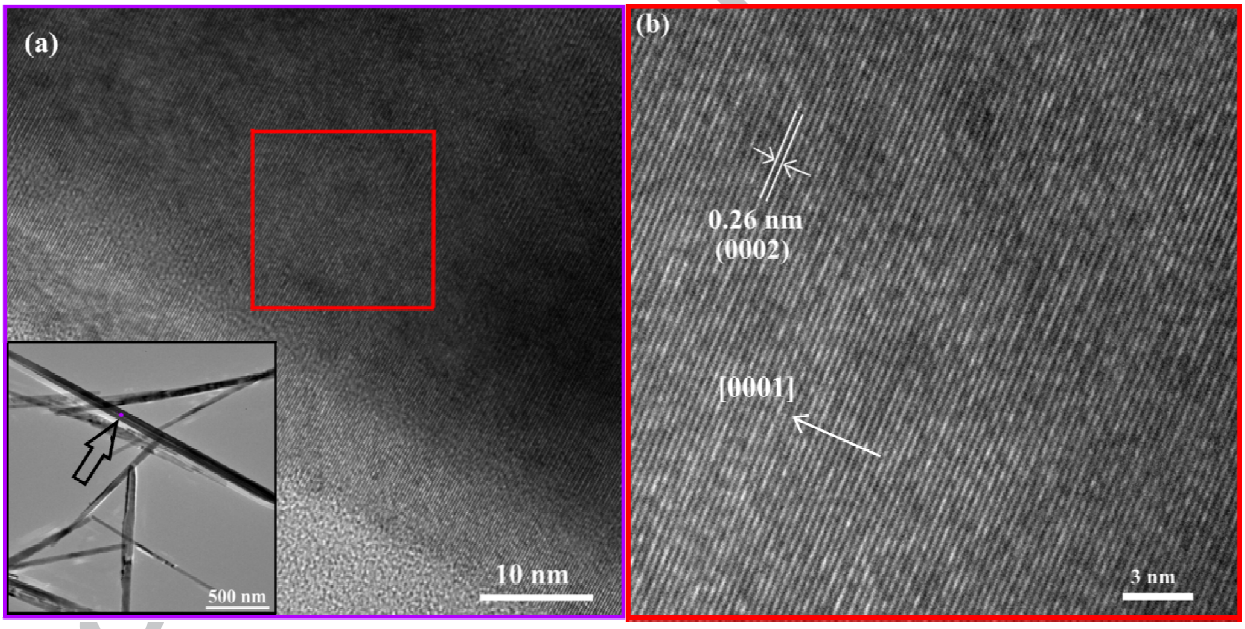

Fig 2. (a) HRTEM image of a ZnO NW. The inset shows the location of the image acquisition. (b) high magnification HRTEM image taken from the area indicated in (a) and showing the distance between the (0002) planes.

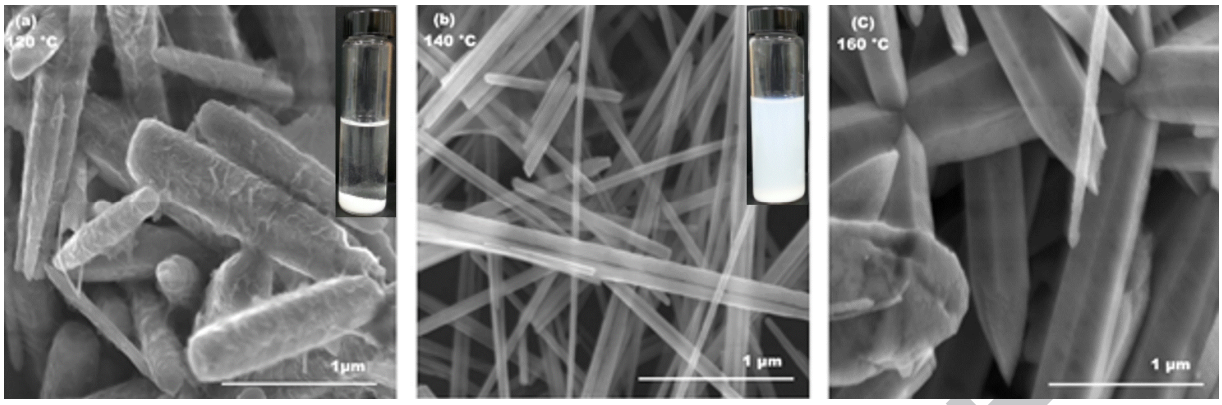

Fig. 3 ZnO NWs grown at (a) 120 °C, (b) 140 °C and (c) 160°C. All other parameters are identical and the three images are recorded at the same magnification. The insets in (a) and (b) show supsension of the rinsed growth products 15 mins after sonication, highlighting the difference in sedimentation rate

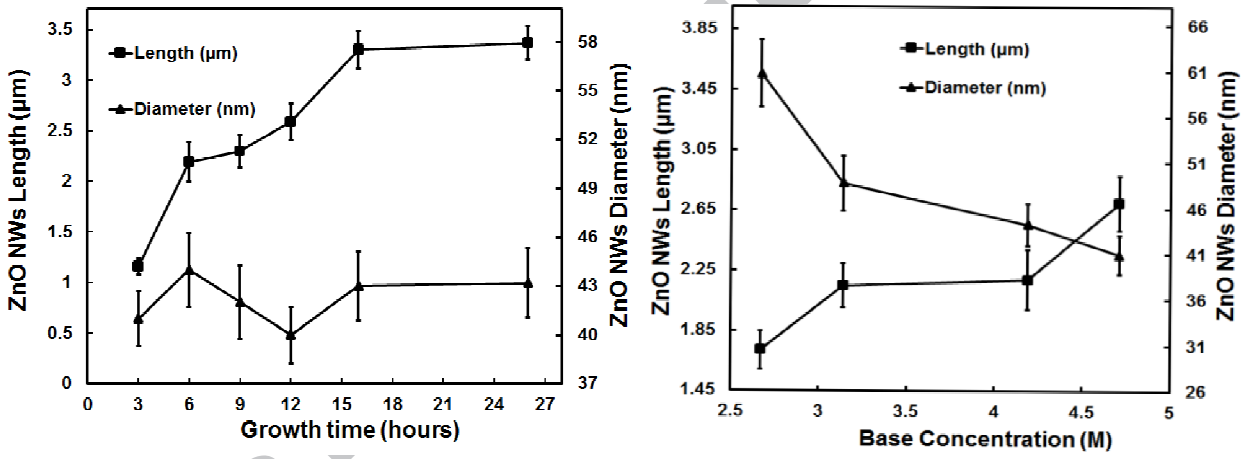

Fig. 4(a) ZnO NWs length and diameter versus growth duration time. NWs are grown at 140°C using a base concentration of 4.193 M. 4(b) ZnO NWs length and diameter versus base (Na_2CO_3) concentration. NWs are grown at the same temperature of 140 °C and for 6 h. Error bars are 2 standard errors wide

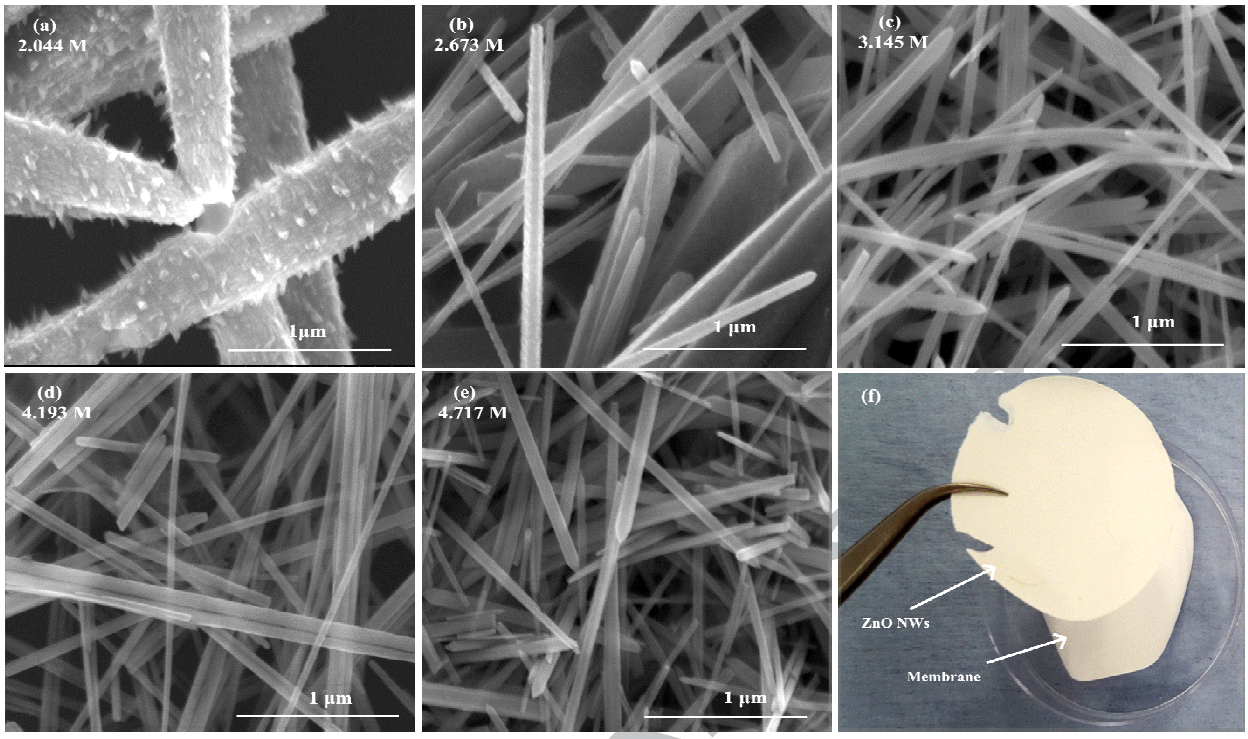

Fig. 5 SEM Images of the ZnO NWs grown at 140 °C for 6 h with base concentrations of Na_2CO_3 of (a) 2.044 M, (b) 2.673 M, (c) 3.145 M, (d) 4.193 and (e) 4.717 M. Images are taken at the same magnification. (g) Filtered and dried ZnO NWs produced from 0.032 M $ZnCl_2$

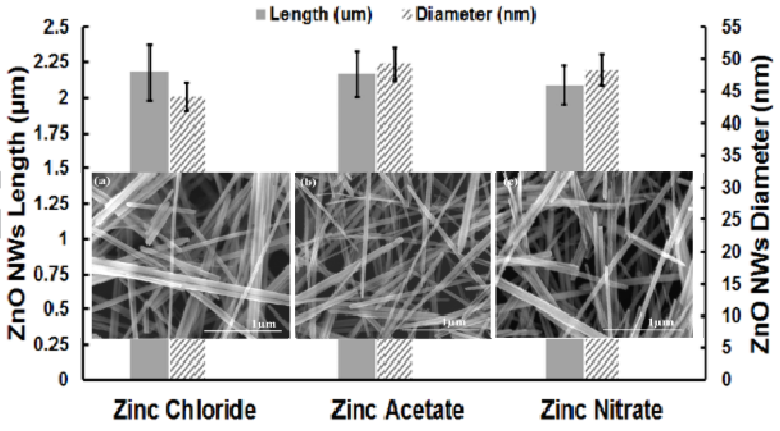

Fig. 6 ZnO NWs SEM images, length and diameter for the three zinc precursors studied. Growth conditions are the same apart from the zinc salt: 140°C, 6 h, 4.193 M Na_2CO_3 and 0.032 M zinc salt.

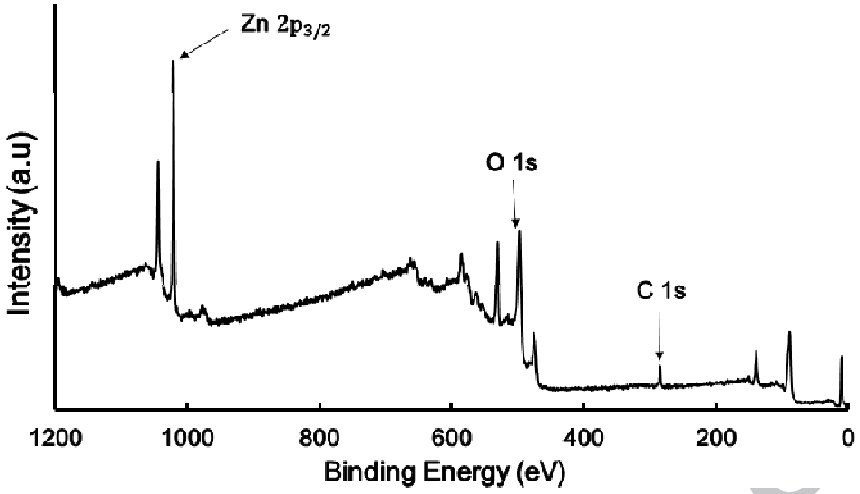

Fig. 7 XPS survey scan of the ZnO NWs

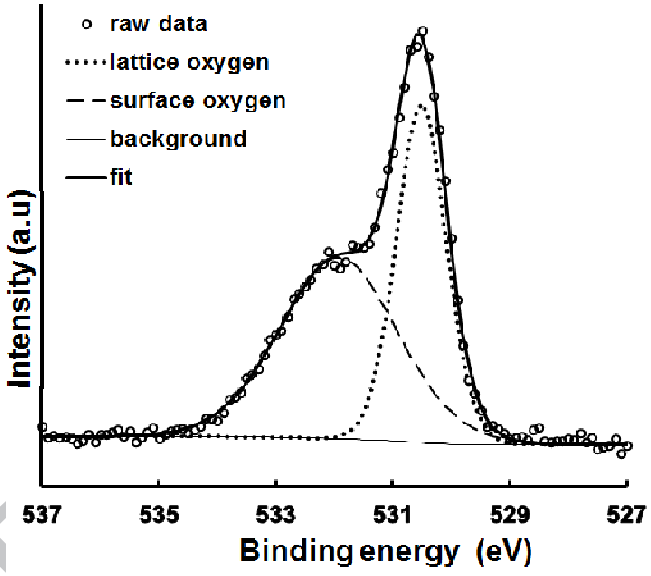

Fig. 8 XPS spectra of the O 1s core level from the as grown NWs. The raw data was fitted with two components and a Shirley background. The two components correspond to the oxygen crystal lattice and the surface oxygen

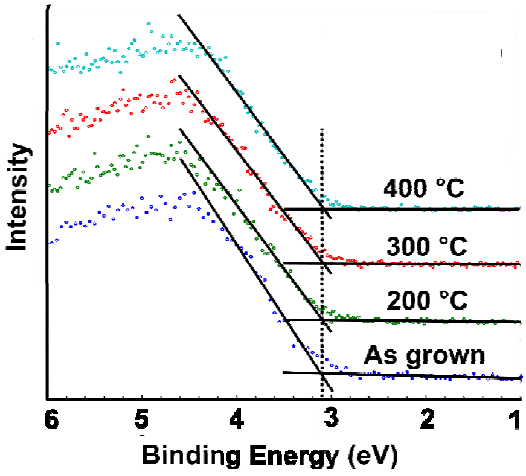

Fig. 9 XPS valence band spectra of ZnO NWs as grown, and annealed at 200, 300 and 400 °C

3.8. Photoluminescence results

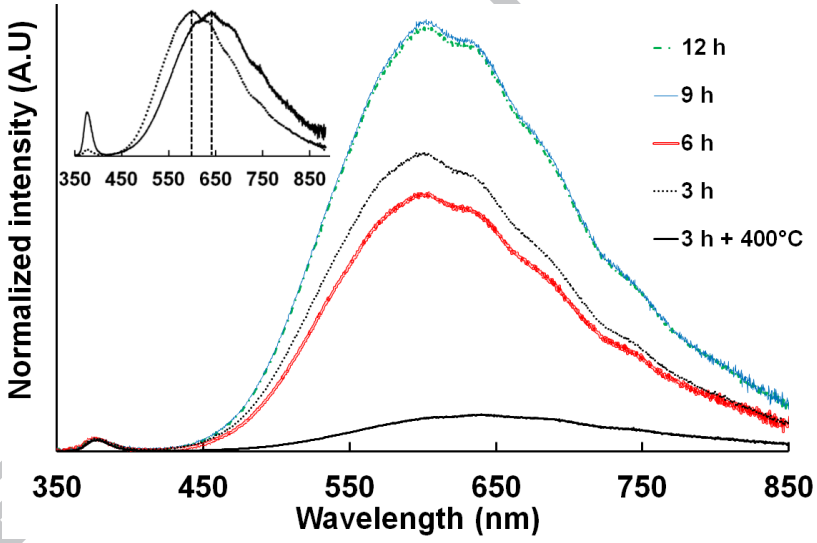

Fig. 10 PL of ZnO NWs grown for 3, 6, 9 and 12 h, and NWs grown for 3 h and subsequently annealed at 400°C. The spectra are normalized to the near band edge peak at 376 nm. The inset shows the spectra of the 3 h NWs, before and after annealing, and are normalised to the deep level band (DLE) intensity to highlight the change in the shape of the DLE band.